Environ Earth Sci (2017)76:379
DOI 10.1007/s12665-017-6706-6

THEMATIC ISSUE

Fiber-optic monitoring of evaporation-induced axial strain of sandstone under ambient laboratory conditions

Yankun Sun[1,2] · Qi Li[1] · Chengkai Fan[1,2] · Duoxing Yang[3] · Xiaochun Li[1] · An Sun[4]

Received: 16 January 2017 / Accepted: 11 May 2017

Abstract This paper presents the fiber-optic monitoring model and scheme for utilizing a fiber Bragg grating (FBG) sensor array to measure relative humidity. The effect of evaporation on reservoir rock involves various physical and chemical reactions under ambient laboratory conditions, which will result in a significant influence on the mechanical properties, especially for the surface of rock blocks in the fields. In this experiment, it was of great importance to better understand the effects induced by deionized water (DIW) evaporation occurring on the surface of a DIW-saturated sandstone core in terms of the induced small strains. The primary objective of this paper is to identify the applicability and feasibility of using the fiber Bragg grating sensors to monitor small strains induced by natural evaporation. This work also brings novel insights into the capability of high-precision measurements to predict the deformation mechanism of outcropped rocks, which often are subjected to natural evaporation. In this work, two arrays of fiber Bragg grating sensors were employed in the real-time monitoring of strain changes along the axial surface of a cylindrical sandstone core and to record the potential implications of the wavelength shifts induced by the evaporation factor. The experimental results could provide novel insights into the influences of natural evaporation on a rock monitored by FBG sensing technology under ambient laboratory conditions.

Keywords Fiber Bragg gratings (FBG) · Sensing arrays · Evaporation · Axial strain · Sandstone · Relative humidity

Introduction

Evaporation is a type of liquid vaporization that occurs at the surface of a liquid as the fluid enters into a gaseous phase that is not saturated with the evaporating substance. Evaporation is a fundamental part of the water cycle and constantly occurs throughout nature. The evaporation impact phenomenon widely exists in geomaterials, infrastructures, metals, geotechnical instrumentations, etc., especially the strong impact on rock-soil mass under various shallow geological environments (Kong et al. 2012). Due to its common occurrence, it is easy for people to overlook the impacts of evaporation. However, evaporation is one physical phenomenon that might require deeper investigation into its mechanism. Having a precise knowledge of evaporation processes on rock surfaces is important in addressing and explaining many practical problems in geotechnical and geoenvironmental engineering (Xie et al. 2014).

Because the magnitude of strains induced by evaporation is much smaller than that from strains induced by drying of deformable two-phase media (liquid–solid

This article is part of a Topical Collection in Environmental Earth Sciences on "Subsurface Energy Storage II," guest edited by Zhonghe Pang, Yanlong Kong, Haibing Shao, and Olaf Kolditz.

✉ Qi Li
qli@whrsm.ac.cn

[1] State Key Laboratory of Geomechanics and Geotechnical Engineering, Institute of Rock and Soil Mechanics, Chinese Academy of Sciences, Wuhan 430071, China

[2] University of Chinese Academy of Sciences, Beijing 100049, China

[3] Key Laboratory of Crustal Dynamics, Institute of Crustal Dynamics, China Earthquake Administration, Beijing 100085, China

[4] College of Civil Engineering, Southeast University, Nanjing 210096, China

Published online: 23 May 2017

coupling reactions), most previous studies focus primarily on drying-induced stress/strain responses of the varying material properties under different drying conditions. A substantial number of previous studies have been reported in the field of evaporation- or drying-induced performance variations in deformable media. Certain notable contributions include the field and laboratory investigations of (Soe et al. 2009, 2010; Wasantha et al. 2013; Xu et al. 2013b; Osada 2014; Roels et al. 2014; Wu et al. 2015; Prime et al. 2016; Sengupta and Tirumkudulu 2016; Tang et al. 2016; Villalobos 2016); the theoretical and numerical developments of (Mihoubi and Bellagi 2009a, b; Hammouda and Mihoubi 2014; Roels et al. 2014; Liang et al. 2015; Wang and Wei 2015; Heydari and Khalili 2016); and the evaporation-induced deformation studies of (van Dam and Feddes 2000; El-Sayed et al. 2016; Hu et al. 2016; Zuo et al. 2016) for saturated–unsaturated geomaterials.

However, all these contributions have been restricted to the study of drying processes in the context of artificial conditions. Indeed, there are very few experiments centering on the mechanical behaviors of deformable media under ambient conditions, particularly with explicit consideration of strain variations in core-scale reservoir rock simulated in situ experiments (Xu et al. 2007; Huang et al. 2012). To acquire precise information of small strains, there is an urgent need for high-resolution monitoring techniques (Xu et al. 2013a).

Optical fiber Bragg grating (FBG) sensors have been established as a promising new technology for advancing state-of-the-art in situ structural health monitoring of various geostructures. The primary advantages of FBGs over other electric/optical sensors schemes are their accuracy, sensitivity, small size, low cost, easy installation, immunity to electromagnetic interference (EMI), wavelength multiplexing, long-term stability, resistance to harsh environments and embedding capability (Majumder et al. 2008; Kou et al. 2012; Montero et al. 2014). FBG-based sensing technology has been attracted increasing interests from geoscientists and geophysical engineers, and a large number of monitoring studies have been reported in different research fields (Wang and Tang 2010; Mihailov 2012; Lai et al. 2013; Kinet et al. 2014; Lamberti et al. 2015; Sun et al. 2015, 2016a, b; Elshafey et al. 2016).

To date, however, there have been very few relevant investigations concerning the slight mechanical deformations of exposed rocks subjected to various long-term weathering processes. To the best of the authors' knowledge, quantitative experimental investigations into the strain fields in unsaturated sandstone during natural evaporation processes are almost nonexistent. Therefore, this exploratory experiment tentatively conducted under ambient laboratory conditions is of even more significance for obtaining insight into the evaporation-induced deformation behaviors of sandstone cores. Moreover, high-precision, real-time monitoring of the strain variations can be implemented in this laboratory test by employing the FBG-based sensing technology.

The primary objective of the present paper is to introduce a new multichannel, fiber-optic monitoring system based on fiber Bragg grating sensor arrays. This system is applied in a laboratory test for the detection of real-time axial strain variations in a cylindrical sandstone sample under simulated in situ conditions considering the influences of natural evaporation from a new point of view. The experimental first results demonstrate the usefulness and superiorities of this FBG sensing system with ultrahigh dynamic strain resolution. The system can subtly depict the strain history of the sandstone core subjected to the processes of the saturated to unsaturated phases and could potentially provide new insights into evaporation from another perspective.

Principle of FBG sensing technology

FBGs are obtained by creating periodic variations in the refractive index of the optical fiber core (Meltz et al. 1989; Zhu et al. 2014). Figure 1 shows the internal structure of an optical fiber written with an FBG. Light passing through the grating at a particular wavelength is called the Bragg wavelength and is given by

$$\lambda_B = 2n_{\text{eff}}\Lambda \tag{1}$$

where λ_B is the Bragg wavelength, nm (nanometer); n_{eff} is the effective refractive index of the FBG, a dimensionless unit; and Λ is the grating period, nm.

When a thermomechanical load acts on the FBG, the Bragg wavelength shift $\Delta\lambda_B$ is expressed as

$$\begin{aligned}\Delta\lambda_B &= 2\left(\Lambda\frac{\mathrm{d}n_{\text{eff}}}{\mathrm{d}\varepsilon} + n_{\text{eff}}\frac{\mathrm{d}\Lambda}{\mathrm{d}\varepsilon}\right)\varepsilon + 2\left(\Lambda\frac{\mathrm{d}n_{eff}}{dT} + n_{\text{eff}}\frac{\mathrm{d}\Lambda}{\mathrm{d}T}\right)\Delta T \\ &= \lambda_B(1-p_e)\varepsilon + \lambda_B(\alpha+\xi)\Delta T = S_\varepsilon\varepsilon + S_T\Delta T\end{aligned} \tag{2}$$

where ε is the longitudinal strain, με or %; ΔT is the temperature variation, °C; p_e is the effective photo-optic constant of the fiber, 0.22 $\mu\varepsilon^{-1}$; and α and ξ denote the strain and temperature coefficients, $0.78 \times 10^{-6}\ \mu\varepsilon^{-1}$ and $6.67 \times 10^{-6}\ ^\circ\mathrm{C}^{-1}$, respectively.

For a temperature-free FBG, the Bragg wavelength shift is only dependent on the applied strain, described by

$$\Delta\lambda_B/\lambda_0 = (1-p_e)\varepsilon = S_\varepsilon\varepsilon \approx 0.78\varepsilon \tag{3}$$

where $\Delta\lambda_B$ is the wavelength difference of the present compared to the original Bragg wavelength λ_0, and p_e is an effective strain-optic constant, 0.22 $\mu\varepsilon^{-1}$. Thus, for

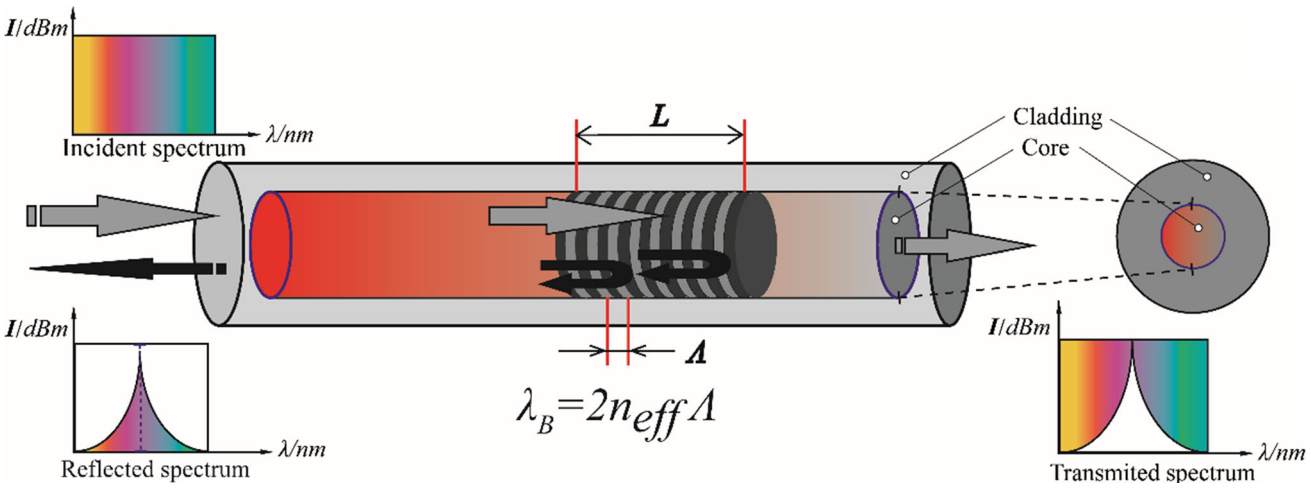

Fig. 1 Schematic diagram of the FBG sensor in a bare optical fiber

measurement of strain, the essence of FBG-based sensing is to accurately identify $\Delta\lambda_B$.

Materials and methods

Test equipment

The whole apparatus employed in the test consists of three main parts: the FBG sensing arrays, signal interrogation and display, and sandstone specimen, as depicted in Fig. 2. The FBG sensing system is composed of two FBG sensor arrays, which are written by three gratings (A1–A3) into each bare fiber, and one single FBG (A0) applied for temperature compensation. In addition to these gratings, there are custom-built sensors in the specialized FBG apparatus. Certain key parameters of the custom FBG sensing arrays used in this test are given in Table 1.

The FBG-reflected signal is demodulated by a highly integrated 4-channel (4C) FBG interrogator box with an adjustable sampling frequency ranging from 1 to 500 Hz, and its principal components are shown in Fig. 2. For this test, the wavelength data were collected continuously at 0.1-s intervals and then written to a text file.

Seven FBG sensors were installed to monitor the dynamic strain induced by evaporation. Among these sensors, six ones belong to the two sensor arrays linking into Ch2 and Ch4 and were pasted approximately parallel to the axial symmetry onto the rock. The array connecting Ch2 was glued with DP100 Clear epoxy adhesive, while the associated Ch4 array was adhered with silicon along the surface of the intact rock to measure the vertical strain. Sensing units were arrayed at equal intervals in one single optical fiber, while the gratings in Ch2 were arrayed in parallel with those in Ch4. The two arrays also have certain differences, as listed in Table 2. A single FBG sensor (A0)

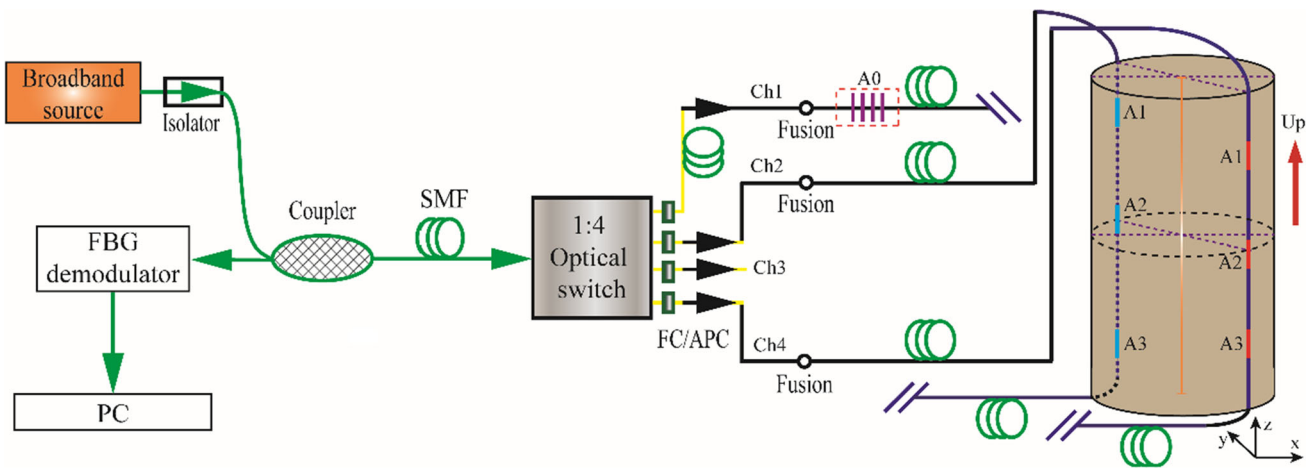

Fig. 2 Experimental setup of the FBG sensor arrays for dynamic strain detection on the sandstone specimen

Table 1 Specifications of customized FBG sensing arrays

Parameters	λ_B	λ_B tolerance	Reflectivity	3 dB bandwidth	Recoating	L	Fiber type	Pigtail	Number
Units	nm	nm	%	nm	–	mm	–	m	Pcs
Value	1510–1590	±0.5	1–99	0.1–1.0	Acrylate	10	SMF-28e$^+$	1	3

Reflectivity: $R\% = 1 - 10^{(T\ (\mathrm{dB})/10)}$. Three decibel bandwidth: called the full width at half maximum (FWHM). FBG width at 50% (−3 dB) from FBG maximum reflectivity, measured from reflection spectra. L: FBG length or grating length. Pcs: an abbreviation of pieces, meaning specifically the number of FBG sensors embedded into an array

Table 2 Differences between the two arrays used in our experiments

Channel	Label	λ_{B0} (nm)	Δ (mm)	Installation mode	Glue type
Ch1	Ch1-Temp.	1564.1		Without external forces	–
	Ch2-1 (A1)	1541.0		Pretension	
Ch2	Ch2-2 (A2)	1543.0	42	Surface mounted	Epoxy resin
	Ch2-3 (A3)	1546.0			
	Ch4-1 (A1)	1550.5		Pretension	
Ch4	Ch4-2 (A2)	1553.5	30	Surface mounted	Silicone
	Ch4-3 (A4)	1556.5			

was mounted to detect the air temperature in the laboratory and to remove the cross-sensitivity effect.

Specimen preparation

The cylindrical sandstone sample was collected from a block of rock outcrop in a quarry in southeast Sichuan Basin, China. The stratigraphic horizon was the major gas and oil production layer in the Penglaizhen formation and belonged to the upper Jurassic age. The core specimen was processed into a right circular cylinder with a length of 125 mm and a diameter of 50 mm. The primary physical properties of the sandstone used in this study, based on bulk rock analysis, are reported in Table 3. The sandstone blocks were first cored according to ASTM recommended standards, and both ends of each specimen were then carefully ground to produce flat parallel surfaces to eliminate the end effect.

Experimental setup

The entire experimental setup was composed of the sandstone core and the optical fiber sensor (OFS) measurement system. The OFS system consisted of an integrated optical spectrum interrogator that was controlled by a personal computer (PC). The FBG sensor arrays were wired to a data acquisition box in different channels and were controlled using a computer workstation. Two FBG sensor arrays with a total of 3 multiplexed gratings for each were connected to the interrogator with which the strain measurements were taken. A single fiber adjacent to the specimen surface was adopted to record the wavelength shift induced by ambient temperatures, so it was left mechanically free without being adhered to the sample. The two sensor arrays had different grating intervals of 30 and 42 mm and were adhered to the rock surfaces at axisymmetric locations of the core. The array linked to Ch2 was recoated with quick set DP100 Clear, a two-part epoxy adhesive (3 M^{TM} Company, USA) with a curing cycle of 2 h at 80 °C, to improve the mechanical strength and coupling stiffness of the FBG sensors epoxied to the sandstone core. The other array with the grating interval of 42 mm was bonded to the rock surface using KE-45-T silicone resin (Shin-Etsu Chemical Co., Ltd, Japan). In addition to the different glue selection schemes, the attachment parts required attention before setting up the experiment.

Table 3 Certain physical properties of the sandstone specimen

Properties	Volume	Specific gravity	Water content	Porosity	Permeability	σ_C	σ_τ	E	ν
Units	cm^3	–	wt %	%	nD	GPa	GPa	GPa	–
Value	194.75	2.74	1.12	8.32	0.49	28.3	5.82	20.31	0.21

Experimental procedure

To improve the real-time monitoring of the processes of the evaporation experiment, a novel optical sensing technology based on FBG sensors was employed to record the surface strain readings from the core, which was in the state of water loss caused by natural evaporation.

In consideration of sufficient complexity and reproducibility, the experiment steps are outlined below:

- The sandstone sample was first polished to be even and smooth using abrasive paper, and then, it was cleaned of surface grains and dust. Where necessary, the rock surface was scrubbed with deionized water (DIW).
- The core was vacuumed for at least 24 h to ensure that no air remained inside the pore throats. Next, the core was saturated with the prepared DIW for at least 48 h. The core was then placed in an oven at 75 °C and stabilized for 8 h.
- The two sensor arrays with the grating lengths of 30 and 42 mm were adhered to the specimen surface along the axial direction using DP100 epoxy resin and silicone, respectively. Simultaneously, the array adapters were connected to the FBG sensing interrogator controlled by data acquisition software. Then, the specimen was cured for 24 h at room temperature.
- The sample with the FBG sensors was submerged into DIC solution for 48 h to saturate it again fully. Then, the FBG-bonded specimen was laid in a sealed cabinet, while the interrogator began to operate with the sampling frequency of 10 Hz, and the FBG temperature sensor was linked to Ch1.
- The readings from the different sensors were exported in Excel format, processed and displayed using the corresponding software for further analysis and interpretations.

For the packaging technique of the FBG strain sensor arrays, it may be noted that in most cases, the uncoated single mode fiber has the highest precision, approximately 0.5 pm per microstrain. Therefore, great care was exercised in adhering the grating elements onto the specimen. The strain and temperature sensitivity used in this study were $S_\varepsilon = 1.2$ pm/με and $S_T = 13.0$ pm/°C, respectively.

Results and discussion

The small strains of the sandstone specimen exposed to the ambient environment were measured by the multichannel FBG strain sensor arrays. The evaporation experiments were carried out to monitor dynamic strains during the processes of saturated–unsaturated sandstone rock. The results were extrapolated to explain the elaborate mechanisms of outcropping rocks in natural evaporation environments, e.g., the strength reduction of rocky constructions and the periodic tidal actions toward the nearshore rock masses and buildings.

Data from the sensors were acquired at a sampling rate of 10 Hz and presented with the relative strain to monitor the evaporation procedures. Before carrying out the FBG sensing array evaporation tests, the sensors were debugged numerous times at atmospheric pressures and temperature.

During the initial 4000 s of the test, shown in Fig. 4, the surface strain induced by evaporation reached approximately 750 με for Ch2-1, 1000 με for Ch2-2 and 500 με for Ch2-3, while the strains of Ch4 were approximately 550, 180 and 100 με. After 500 s, the specimen was in a steady state, and the readings of Ch2 and Ch4 were stable. As shown in Fig. 4, the strain varied from 0 to 30 με, which equaled $\Delta T = 2.3$ °C according to the temperature sensitivity of 13 pm/°C. The FBG sensors were employed to record the reflected signals in real-time to quantitatively investigate the evaporation effects on the sample.

The FBG wavelength shifts caused by the temperature changes were insignificant, as depicted in Figs. 4 and 5. This result indicated that the influence of ambient temperature variations on the specimen was negligible. Thus, the following recordings from FBG arrays did not take the temperature effect into account.

Certain slight changes in the strain history for the same levels of the specimen were observed, i.e., strains from Ch2 sensors had higher variations than those from Ch4 sensors. This discrepancy occurs because, although both sensor types were placed at approximately symmetric locations (shown in Fig. 3), the evaporation speed might be a little inhomogeneous on the specimen.

As shown in Fig. 5, strains originating from the three sensors in Ch2 exhibited much stronger fluctuations than those in Ch4. This difference implied that the grating element adhered with DP100 Clear epoxy had a low coupling, which resulted in a very high variance, and a jump even occurred. During the experiment, slight striping emerged in sensor Ch2-2, and obvious stripping occurred in sensor Ch2-3. One possible reason is that during the sample saturation and evaporation, moisture reduced the coupling behavior between the glue and rock particles. Thus, the significant strain changes detected were the strains induced by free water evaporation only on the grating surface, not by water loss from the specimen surface. Therefore, due to the large fluidity of free water, Ch2-2 and Ch2-3 had drastic jumps at irregular intervals.

As shown in Fig. 6, the strain responses underwent consistent drifts with evaporation time. The strain results of the evaporation behavior in the sandstone specimen were acquired after thirteen days. The sensor arrays in Ch2

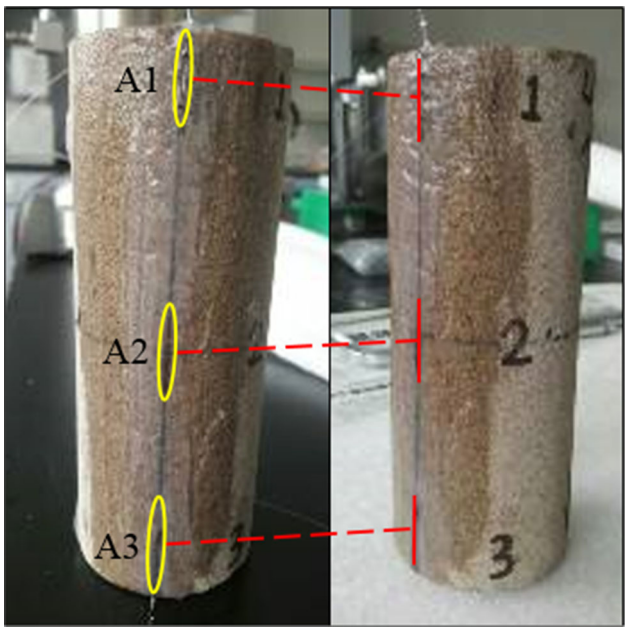

Fig. 3 Photograph of the core specimen and the FBG layout

captured the range of −2 με to 6 με for the evaporation-induced strain, while the sensors attached to Ch4 recorded the surface strains from the other side of the sample.

As evaporation time elapsed, the relative strain tended to be steady. The strains derived from Ch2 and shown in Fig. 6 indicated that the surface adjacent to the grating segments reached a relative evaporation balance, i.e., a small evaporation velocity. It could be inferred that the slight fluctuation from -2με to 6με was noise because the noise in the determination of the Bragg wavelength is less than 10 pm, meaning an SNR better than 12 dB (1.2 pm means 1 με).

After 4 h of evaporation from 11:05 a.m. to 15:15 p.m., the strains remained stable at −40, −5 and −15 με for Ch2-1, Ch2-2, and Ch2-3, respectively, which manifested the inhomogeneity of the evaporation rate at the different sample positions. According to existing knowledge, there are two primary reasons for the observed strain being generated: One is clay content, and the other is the effective stress. The sandstone used in this test had clay content of approximately 12%, so the effective stress became a relatively important factor to study.

According to Terzaghi's law, rock behaves under the control of the summation of stress and pore pressure as follows (Han and Dusseault 2003):

$$\sigma_{ij}^{\text{eff}} = \sigma_{ij} - p\delta_{ij} = E\varepsilon_{ij} \tag{4}$$

where σ_{ij}^{eff} is the effective stress, σ_{ij} is the total stress, p is the pore pressure, δ_{ij} is the Kronecker delta, E is the elastic modulus, and ε_{ij} is the strain induced by the effective stress. The reason to introduce the Kronecker delta is that pore pressure has no effect on the shear stress.

Evaporation lowers the saturation of the sandstone specimen and then reduces the pore pressure, which can cause the effective pressure to increase. Finally, regarding the theoretical consideration of stress-dependent mechanisms, the evaporation led to the occurrence of small strain increments.

Following the test presented in Fig. 6, the authors performed the 16-h experiment. In Ch2, Ch2-1 and Ch2-2, there were almost no changes, while Ch2-3 reached a peak value of 78 με at 9:31 a.m. and then remained constant. It could be deduced that Ch2-3 had completely separated from the rock surface because the AB adhesive was subjected to long-term soaking in DIW, which would gradually weaken the curing.

As shown in Figs. 4, 5, 6 and 7, in Ch4, the relative sensors in Ch4-2 detected the largest change, and the sensor was in the middle of the sample. Therefore, it was easily concluded that the evaporation most affected the middle section of the sample, as the two rock ends had the smallest evaporation area.

Because high rocky buildings have been widely constructed in coastal regions around the globe, it is inevitable that periodic seawater fluctuation, immersion, and evaporation, i.e., the tide, have a significant effect on architecture safety. In the northwest areas of China, intense evaporation has a notable influence on the design, construction, and safety of many geostructures. Therefore, monitoring these structures based on FBG sensing technology is critical to evaluate and assess evaporation impacts.

The quantitative results of the experiment better reveal the implications of evaporation-induced rock mass instability, indicating the potential for long-time monitoring of the impact of natural evaporation and thus guiding engineers and field staff to design timely protection programs, early warning, etc. Additionally, these original data and monitoring schemes can be applied to compensate for the lack of natural evaporation research in the relevant experimental literature.

Conclusions

In summary, we have conducted an experimental study on the application of multichannel FBG sensor arrays for monitoring the evaporation processes of a saturated to unsaturated sandstone specimen under laboratory ambient temperatures. The results illustrate that there is a consistency between the signals recorded and the evaporation interactions under the same operational conditions.

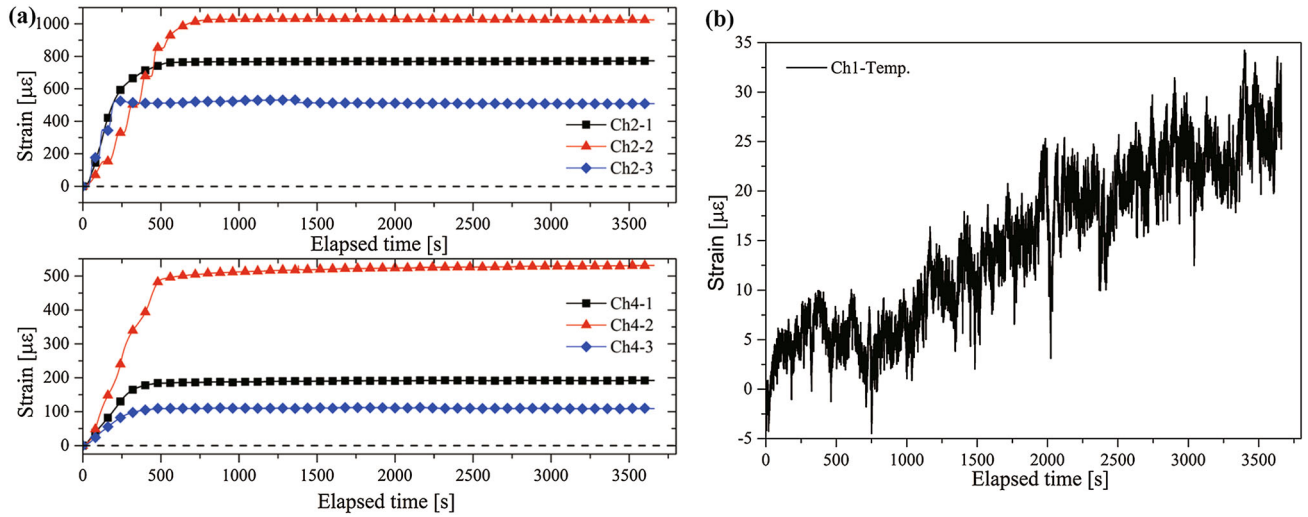

Fig. 4 Strain responses with time on April 29, 2016 (**a**), and the strain variation induced by ambient temperatures in a single fiber (**b**)

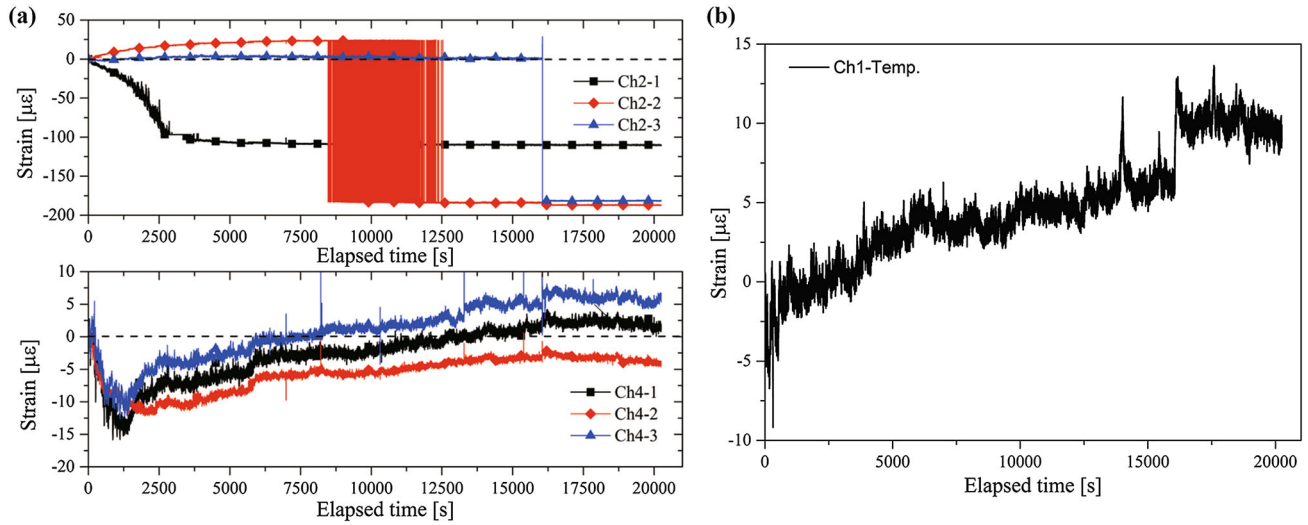

Fig. 5 Strain responses with time on May 1, 2016 (**a**), and the strain variations induced by the ambient temperature in a single fiber (**b**)

Natural evaporation effects on soil and rock masses, particularly on the outcropping rock type, can influence the deformation and mechanical strength of rocky buildings weathered in the long term due to atmospheric precipitation. Therefore, these effects can be diagnosed by analyzing and comparing the strain information measured by the FBG technology, which is adequate for multichannel sensors over time. We have demonstrated the possibility of adhering these sensors at different positions on the core specimen to determine the influence of natural evaporation on surface strains. Further experiments must be conducted to measure absolute evaporation effects on dry and saturated samples under the same conditions and conducted on the precise encapsulation and calibration of FBG sensors during the courses of the tests.

The experience obtained from this study also highlights potential practical difficulties in realizing good coupling between a rock and gratings. This knowledge is undoubtedly useful for defining further work and seeking improvements in both effectiveness and defect detection reliability.

However, the work reported in this paper is the first trial from a new perspective of strain responses induced by natural evaporation processes for a saturated–unsaturated sandstone sample based on the FBG sensing technique. Within the experimental data, certain unexpected results appeared, primarily due to the many factors that influence natural evaporation processes under ambient conditions and the high-sensitivity of FBG sensors in this study. We speculate that the possible error sources were as follows:

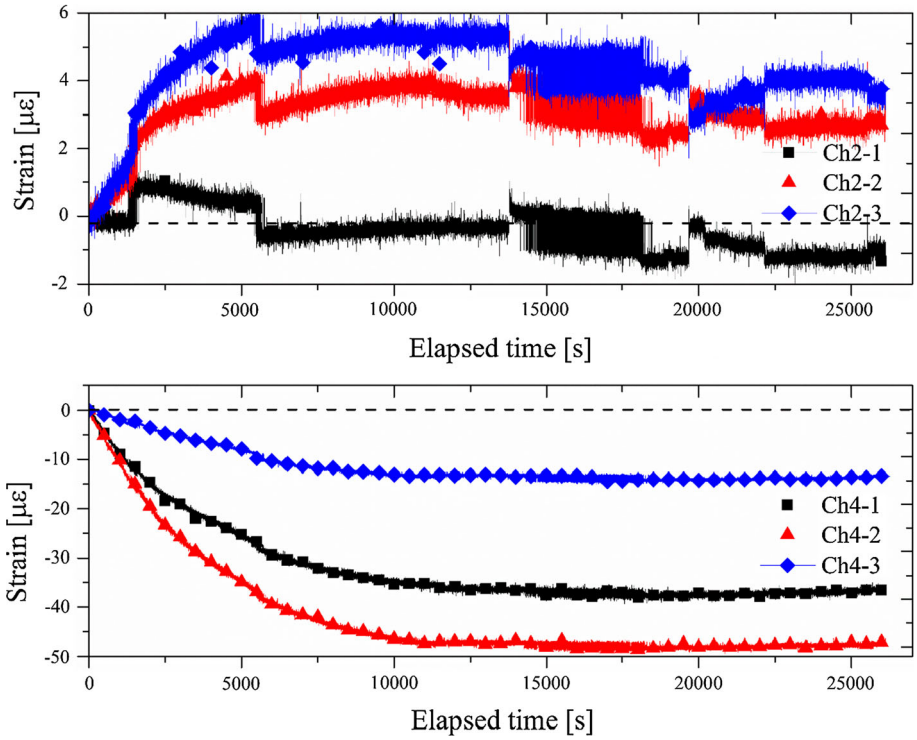

Fig. 6 Strain history of the sandstone surface on May 11, 2016, from 11:05 a.m. to 18:20 p.m.

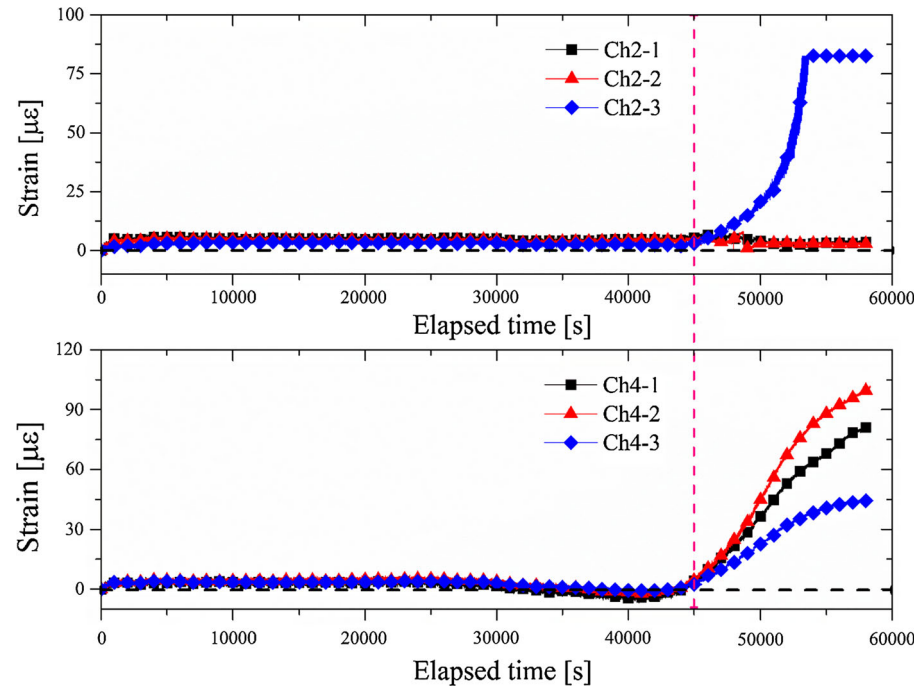

Fig. 7 Strain history of the sandstone surface from 18:31 p.m. on May 11, 2016, to 10:43 a.m. on May 12, 2016

different evaporation rates at different grating locations, various adhesive types, inappropriately adhered components of local FBG sensors in one array, and external environment interferences, such as breeze or vibration. To acquire accurate results induced by evaporation processes, first, we considered temperature effects on the FBG sensors, so the achieved results were calculated as the measured Bragg wavelengths minus the wavelength shift induced by temperature variations to eliminate the cross-sensitivity effect. Second, the whole testing apparatus was kept in relatively quiet surroundings to reduce external disturbance as much as possible. Finally, the achieved values were dependent on evaporation processes and adhesive types. However, for FBG sensors belonging to the

same array (i.e., using the same adhesive), their local strain differences could be explained by unequal evaporation processes. Meanwhile, different overall trends between the two arrays could be ascribed to the different adhesive types. Moreover, for the short-term experiments, the effect of the adhesive parameters on the FBG sensors was slight, particularly in the later evaporation processes. One additional factor to consider was the humidity sensitivity of the main sensing system components. These components of the FBG interrogator were depicted as having a working humidity range of 20–80%, waterproof material for the FBG sensors, whose humidity sensitivity was reflected in the effect induced by natural evaporation on the grating element, and good waterproof ratings for the DP100 Clear epoxy adhesive and silicone. Therefore, the humidity sensitivity of the experimental components primarily lies in the FBG sensors' response to natural evaporation under ambient conditions.

Acknowledgments This work is primarily supported by the National Natural Science Foundation of China (Grant No. 41274111) and partially supported by the Institute of Crustal Dynamics, China Earthquake Administration (Grant No. zdj2016-20). The authors also wish to thank Dr. Xinglin Lei (AIST, Japan) for his valuable advice and suggestions.

References

El-Sayed MMH, Amenumey D, Hennigan CJ (2016) Drying-induced evaporation of secondary organic aerosol during summer. Environ Sci Technol 50(7):3626–3633. doi:10.1021/acs.est.5b06002

Elshafey A, Marzouk H, Gu X, Haddara M, Morsy R (2016) Use of fiber Bragg grating array and random decrement for damage detection in steel beam. Eng Struct 106:348–354. doi:10.1016/j.engstruct.2015.10.046

Hammouda I, Mihoubi D (2014) Comparative numerical study of kaolin clay with three drying methods: convective, convective-microwave and convective infrared modes. Energy Convers Manag 87:832–839. doi:10.1016/j.enconman.2014.07.085

Han G, Dusseault MB (2003) Description of fluid flow around a wellbore with stress-dependent porosity and permeability. J Petrol Sci Eng 40(1–2):1–16. doi:10.1016/s0920-4105(03)00047-0

Heydari M, Khalili K (2016) Investigation on the effect of young's modulus variation on drying-induced stresses. Transp Porous Media 112(2):519–540. doi:10.1007/s11242-016-0664-4

Hu C, Wang Y, Wang W, Liu S, Piao M, Xiao W, Lee X (2016) Trends in evaporation of a large subtropical lake. Theor Appl Climatol. doi:10.1007/s00704-016-1768-z

Huang H, Yang CQ, Wu ZS (2012) Electrical sensing properties of carbon fiber reinforced plastic strips for detecting low-level strains. Smart Mater Struct 21(3):7. doi:10.1088/0964-1726/21/3/035013

Kinet D, Megret P, Goossen KW, Qiu L, Heider D, Caucheteur C (2014) Fiber Bragg grating sensors toward structural health monitoring in composite materials: challenges and solutions. Sensors 14(4):7394–7419. doi:10.3390/s140407394

Kong L, Bai W, Guo A (2012) Effects of cracks on the electrical conductivity of a fissured laterite: a combined experimental and statistical study. Geotech Test J 35(6):1–9. doi:10.1520/GTJ20120070

Kou J-L, Ding M, Feng J, Lu Y-Q, Xu F, Brambilla G (2012) Microfiber-based Bragg gratings for sensing applications: a review. Sensors. 12(7):8861–8876. doi:10.3390/s120708861

Lai M, Karalekas D, Botsis J (2013) On the effects of the lateral strains on the fiber Bragg grating response. Sensors 13(2):2631–2644

Lamberti A, Chiesura G, Luyckx G, Degrieck J, Kaufmann M, Vanlanduit S (2015) Dynamic strain measurements on automotive and aeronautic composite components by means of embedded fiber Bragg grating sensors. Sensors 15(10):27174–27200. doi:10.3390/s151027174

Liang X, Li K, Cai S (2015) Drying-induced deformation in fiber-embedded gels to mimic plant nastic movements. Int J Appl Mech. doi:10.1142/s1758825115500167

Majumder M, Gangopadhyay TK, Chakraborty AK, Dasgupta K, Bhattacharya DK (2008) Fibre Bragg gratings in structural health monitoring—present status and applications. Sens Actuators A 147(1):150–164. doi:10.1016/j.sna.2008.04.008

Meltz G, Morey WW, Glenn WH (1989) Formation of Bragg gratings in optical fibers by a transverse holographic method. Opt Lett 14(15):823–825. doi:10.1364/ol.14.000823

Mihailov SJ (2012) Fiber Bragg grating sensors for harsh environments. Sensors 12(2):1898–1918

Mihoubi D, Bellagi A (2009a) Drying-induced stresses during convective and combined microwave and convective drying of saturated porous media. Dry Technol 27(7–8):851–856. doi:10.1080/07373930902988122

Mihoubi D, Bellagi A (2009b) Stress generated during drying of saturated porous media. Transp Porous Media 80(3):519–536. doi:10.1007/s11242-009-9378-1

Montero A, Aldabaldetreku G, Durana G, Jorge I, Sáez de Ocáriz I, Zubia J (2014) Influence of humidity on fiber Bragg grating sensors. Adv Mater Sci Eng. doi:10.1155/2014/405250

Osada M (2014) Drying-induced deformation characteristics of rocks. In: 8th Asian rock mechanics symposium. International Society for Rock Mechanics, Sapporo, Japan

Prime N, Levasseur S, Miny L, Charlier R, Leonard A, Collin F (2016) Drying-induced shrinkage of boom clay: an experimental investigation. Can Geotech J 53(3):396–409. doi:10.1139/cgj-2015-0099

Roels SM, Ott H, Zitha PLJ (2014) M-ct analysis and numerical simulation of drying effects of CO_2 injection into brine-saturated porous media. Int J Greenh Gas Control 27:146–154. doi:10.1016/j.ijggc.2014.05.010

Sengupta R, Tirumkudulu MS (2016) Dynamics of cracking in drying colloidal sheets. Soft Matter 12(13):3149–3155. doi:10.1039/c5sm03008k

Soe AKK, Osada M, Takahashi M, Sasaki T (2009) Characterization of drying-induced deformation behaviour of Opalinus Clay and tuff in no-stress regime. Environ Geol 58(6):1215–1225. doi:10.1007/s00254-008-1616-2

Soe AKK, Osada M, Win TTN (2010) Drying-induced deformation behaviour of Shirahama sandstone in no loading regime. Eng Geol 114(3–4):423–432. doi:10.1016/j.enggeo.2010.06.001

Sun Y, Li Q, Li X, Yang D (2015) Progress on real-time monitoring in oil and gas industry based with fiber Bragg grating. Sci Technol Rev 33(13):84–91. doi:10.3981/j.issn.1000-7857.2015.13.014

Sun Y, Li Q, Yang D, Fan C, Sun A (2016a) Investigation of the dynamic strain responses of sandstone using multichannel fiber-optic sensor arrays. Eng Geol 213:1–10. doi:10.1016/j.enggeo.2016.08.008

Sun Y, Li Q, Yang D, Liu X (2016b) Laboratory core flooding experimental systems for CO_2 geosequestration: an updated review over the past decade. J Rock Mech Geotech Eng 8(1):113–126. doi:10.1016/j.jrmge.2015.12.001

Tang C-S, Wang D-Y, Shi B, Li J (2016) Effect of wetting-drying cycles on profile mechanical behavior of soils with different initial conditions. CATENA 139:105–116. doi:10.1016/j.catena.2015.12.015

van Dam JC, Feddes RA (2000) Numerical simulation of infiltration, evaporation and shallow groundwater levels with the richards equation. J Hydrol 233(1–4):72–85. doi:10.1016/S0022-1694(00)00227-4

Villalobos G (2016) Acoustic emission signals resulting from the drying-induced fractures of *Phyllostachys pubescens* bamboo: evidence of scale free phenomena. Wood Sci Technol 50(3):489–501. doi:10.1007/s00226-016-0798-0

Wang J-N, Tang J-L (2010) Feasibility of fiber Bragg grating and long-period fiber grating sensors under different environmental conditions. Sensors 10(11):10105–10127

Wang G, Wei X (2015) Modeling swelling–shrinkage behavior of compacted expansive soils during wetting-drying cycles. Can Geotech J 52(6):783–794. doi:10.1139/cgj-2014-0059

Wasantha PLP, Darlington WJ, Ranjith PG (2013) Characterization of mechanical behaviour of saturated sandstone using a newly developed triaxial apparatus. Exp Mech 53(5):871–882. doi:10.1007/s11340-012-9690-5

Wu Z, Wong HS, Buenfeld NR (2015) Influence of drying-induced microcracking and related size effects on mass transport properties of concrete. Cem Concr Res 68:35–48. doi:10.1016/j.cemconres.2014.10.018

Xie H, Li X, Fang Z, Wang Y, Li Q, Shi L, Bai B, Wei N, Hou Z (2014) China's carbon geological utilization and storage: current status and perspective. Acta Geotech 9(1):7–27. doi:10.1007/s11440-013-0277-9

Xu B, Chen G, Wu ZS (2007) Parametric identification for a truss structure using axial strain. Comput Aided Civil Infrastruct Eng 22(3):210–222. doi:10.1111/j.1467-8667.2007.00467.x

Xu D-S, Borana L, Yin J-H (2013a) Measurement of small strain behavior of a local soil by fiber Bragg grating-based local displacement transducers. Acta Geotech 9(6):935–943. doi:10.1007/s11440-013-0267-y

Xu Y, German GK, Mertz AF, Dufresne ER (2013b) Imaging stress and strain in the fracture of drying colloidal films. Soft Matter 9(14):3735–3740. doi:10.1039/c3sm27912j

Zhu HH, Shi B, Yan JF, Zhang J, Zhang CC, Wang BJ (2014) Fiber Bragg grating-based performance monitoring of a slope model subjected to seepage. Smart Mater Struct 23(9):12. doi:10.1088/0964-1726/23/9/095027

Zuo HC, Chen BL, Wang SX, Guo Y, Zuo B, Wu LY, Gao XQ (2016) Observational study on complementary relationship between pan evaporation and actual evapotranspiration and its variation with pan type. Agric For Meteorol 222:1–9